Pflügers Archiv - European Journal of Physiology
https://doi.org/10.1007/s00424-020-02414-0

ORIGINAL ARTICLE

Electromechanical coupling of the Kv1.1 voltage-gated K^+ channel is fine-tuned by the simplest amino acid residue in the S4-S5 linker

Sonia Hasan[1] · Alfredo Megaro[2] · Marta Cenciarini[2] · Lorena Coretti[2] · Fabio Massimo Botti[2] · Paola Imbrici[3] · Harry W. M. Steinbusch[4] · Therese Hunter[5] · Gary Hunter[5] · Mauro Pessia[5,6] · Maria Cristina D'Adamo[5]

Received: 30 April 2020 / Revised: 27 May 2020 / Accepted: 3 June 2020

Abstract

Investigating the *Shaker*-related K^+ channel Kv1.1, the dysfunction of which is responsible for episodic ataxia 1 (EA1), at the functional and molecular level provides valuable understandings on normal channel dynamics, structural correlates underlying voltage-gating, and disease-causing mechanisms. Most studies focused on apparently functional amino acid residues composing voltage-gated K^+ channels, neglecting the simplest ones. Glycine at position 311 of Kv1.1 is highly conserved both evolutionarily and within the Kv channel superfamily, is located in a region functionally relevant (the S4-S5 linker), and results in overt disease when mutated (p.G311D). By mutating the G311 residue to aspartate, we show here that the channel voltage-gating, activation, deactivation, inactivation, and window currents are markedly affected. In silico, modeling shows this glycine residue is strategically placed at one end of the linker helix which must be free to both bend and move past other portions of the protein during the channel's opening and closing. This is befitting of a glycine residue as its small neutral side chain allows for movement unhindered by interaction with any other amino acid. Results presented reveal the crucial importance of a distinct glycine residue, within the S4-S5 linker, in the voltage-dependent electromechanical coupling that control channel gating.

Keywords Episodic ataxia type 1 · Kv1.1 · Kv · S4-S5 linker · *KCNA1* · *Xenopus laevis*

Abbreviations

EA1	Episodic ataxia type 1
I	Current
Kv	Potassium voltage-gated channel
$Kv1.1_{WT}$	Wildtype potassium 1.1 voltage-gated channel
$Kv1.1_{G311D}$	Mutant potassium voltage-gated channel
$Kv1.1_{WT/G311D}$	Heteromeric wildtype and mutant potassium voltage-gated channel
PD	Pore domain
PPM	Prediction of proteins in membrane
S	Segment
TEVC	Two-electrode voltage-clamp
V	Voltage
VSD	Voltage-sensing domain
WT	Wildtype

This article is part of the special issue on Channelopathies: from mutation to diseases in Pflügers Archiv—European Journal of Physiology

✉ Maria Cristina D'Adamo
cristina.dadamo@um.edu.mt

[1] Department of Physiology, Faculty of Medicine and Surgery, Kuwait University, 13110 Safat, Kuwait

[2] Department of Experimental Medicine, Section of Physiology and Biochemistry, School of Medicine, University of Perugia, Perugia, Italy

[3] Department of Pharmacy-Drug Sciences, University of Bari Aldo Moro, Bari, Italy

[4] University of Maastricht, Minderbroedersberg 4-6, 6211 LK Maastricht, Netherlands

[5] Department of Physiology & Biochemistry, Faculty of Medicine & Surgery, University of Malta, Msida MSD 2080, Malta

[6] Department of Physiology, United Arab Emirates University, Al Ain, United Arab Emirates

Introduction

The passage of K^+ ions through voltage-gated potassium (Kv) channels depends on conformational changes that occur in response to a variation in transmembrane potential. It is well accepted that out of the 6 transmembrane segments of a channel's α-subunit (Fig. 1a), the first four (S1-S4) function as the

Published online: 23 June 2020

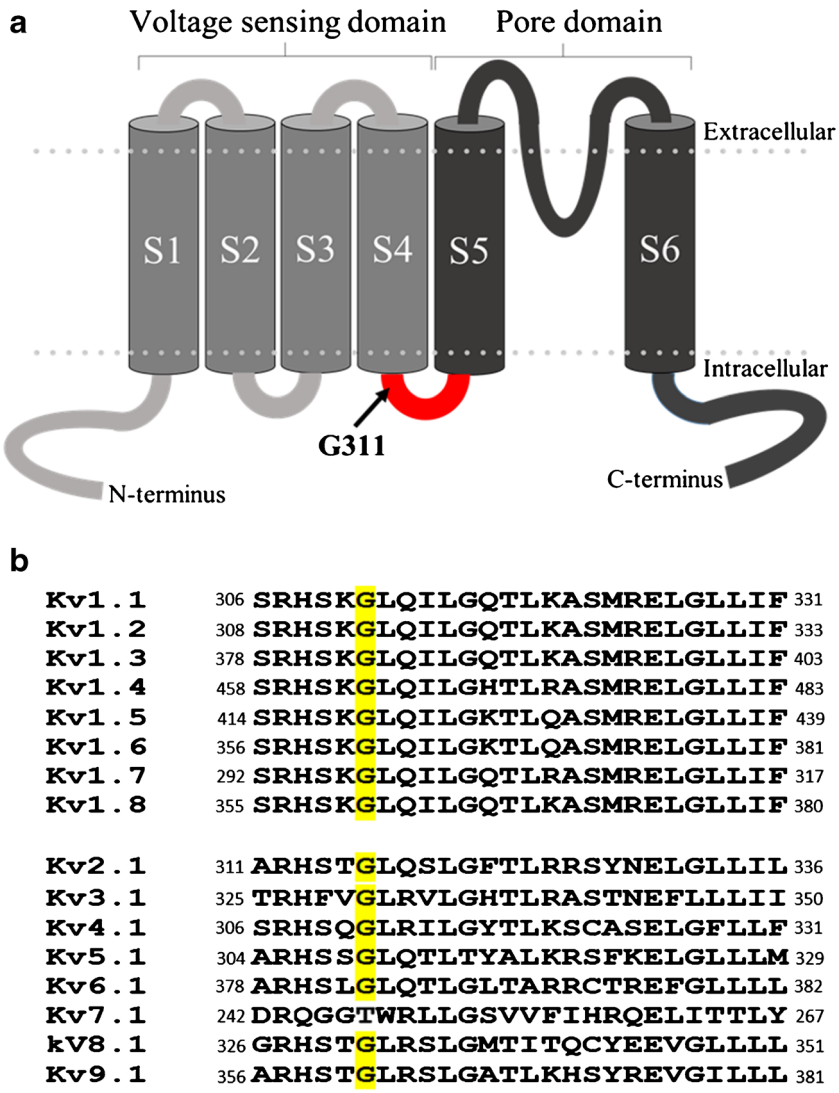

Fig. 1 **a** Schematic model of the Kv1.1 subunit showing the G311 residue within the S4-S5 linker (red) that links the voltage sensing domain to the pore domain. **b** MUSCLE 3.6 was used to obtain an amino acid alignment of different Kv channels. Alignment shows the G311 residue (highlighted) is almost completely conserved in various Kv channels

voltage-sensing domain (VSD). The other two segments, the S5 and S6 helices, and the P loop between them make up the pore domain (PD) that determines the channel's potassium selectivity and through which K^+ ions flow. The VSD is connected to the PD by the S4–S5 linker, which is suggested to be responsible for electromechanical coupling [14, 18]. A Kv channel is made of four such α-subunits. While the channel remains closed during membrane hyperpolarization, depolarization results in the S4 helix of each subunit to move 6–8 Å outward through the membrane [11]. It particularly does so because of the presence of a regular pattern of positively charged amino acids within it. Movement of the S4 sensor would pull on the S4-S5 linker resulting in a structural rearrangement of the PD, the outcome of which is the opening of the channel pore. The amphipathic α-helical S4-S5 linker is comprised of about 14 amino acid residues (region 310 to 324) and is the critical and direct binding site for anesthetics [6]. Despite the linker's strategic position within the channel, its function has been relatively overlooked.

Episodic ataxia type 1 (EA1) is an inherited Kv1.1 α-subunit channelopathy characterized by drastic attacks of ataxia and myokymia [10]. Currents that pass through Kv1.1 are crucial for normal neuronal membrane potentials, excitability, action potential threshold, action potential frequency and neurotransmitter release [2, 13]. Heterozygous point mutations in the Kv1.1 gene (*KCNA1*), located on chromosome 12p13, that result in dysfunctional Kv1.1-containing channels alter these membrane properties resulting in EA1 symptoms [8, 9].

The clinical case of an EA1 patient with a G311D mutation within the S4-S5 linker of the Kv1.1 α-subunit has been recently described in our previous study [12]. The biophysical properties of this novel mutation were, however, not assessed. The importance of this residue is evident in its high conservation, being evolutionary preserved in distinct species as well as amongst the different Kv channels of the *Shaker*, *Shal*, *Shaw*, and *Shab* families (Fig. 1b). All voltage-gated potassium channels have generally the same mechanism for voltage-

sensing and gating that rely on the presence of certain conserved residues. The fact that a human channelopathy results from mutations of the glycine located at the position 311 strongly suggests that this distinct residue may play an important role in channel gating.

In this present study, we focus on the effect of a $Kv1.1_{G311}$ mutation on Kv1.1's voltage-dependence and kinetics. Our results provide insights on a distinct requirement for glycine in interactions controlling the conformational dynamics occurring at the level of the S4-S5 linker that opens Kv channels, electromechanically.

Results

Changes in voltage-dependence of activation and inactivation, and on window current

Oocytes injected with WT RNA showed typical whole-cell delayed rectifying currents upon depolarization. The mutation remarkably reduced Kv1.1 current amplitudes (Fig. 2a) like that reported previously in Karalok et al. [12]. Oocytes injected with homomeric $Kv1.1_{G311D}$ RNA had mean currents significantly lower (22 ± 2 μA measured at + 60 mV, $n = 8$, $p < 0.005$) than that of homomeric $Kv1.1_{WT}$ currents (60 ± 8 μA, 60 mV, $n = 8$). Injecting oocytes with a 1:1 heteromeric mix of Kv1.1WT and Kv1.1G311D channels in the same amount of RNA as in the homomeric experiments resulted in a mean current ($Kv1.1_{WT/G311D} = 36 \pm 4$ μA, $n = 8$, $p < 0.05$) reduction of 40%. This suggests the mutation effect is not dominant negative.

To test the voltage-dependence of Kv1.1 current activation, tail currents were elicited at − 50 mV after pre-pulse commands of 200 ms from − 80 to + 80 mV. Tail current peak amplitudes were plotted as pre-pulse potential function and fitted with the Boltzmann function $I(V) = 1/\{1 + \exp[(V_{0.5} - V)/k]\}$, where $V_{0.5}$ is the half-maximal voltage, and k the slope factor. The mutation G311D shifted the current-voltage (I/Imax – V) curves of both homomeric and heteromeric channels to more positive potentials (Fig. 2b). This rightward shift resulted in a significant change in $V_{0.5}$ of activation from -28 ± 0.8 to 14 ± 2.8 mV ($p < 0.0001$, $n = 24$) for homomeric $Kv1.1_{G311D}$ channels, and

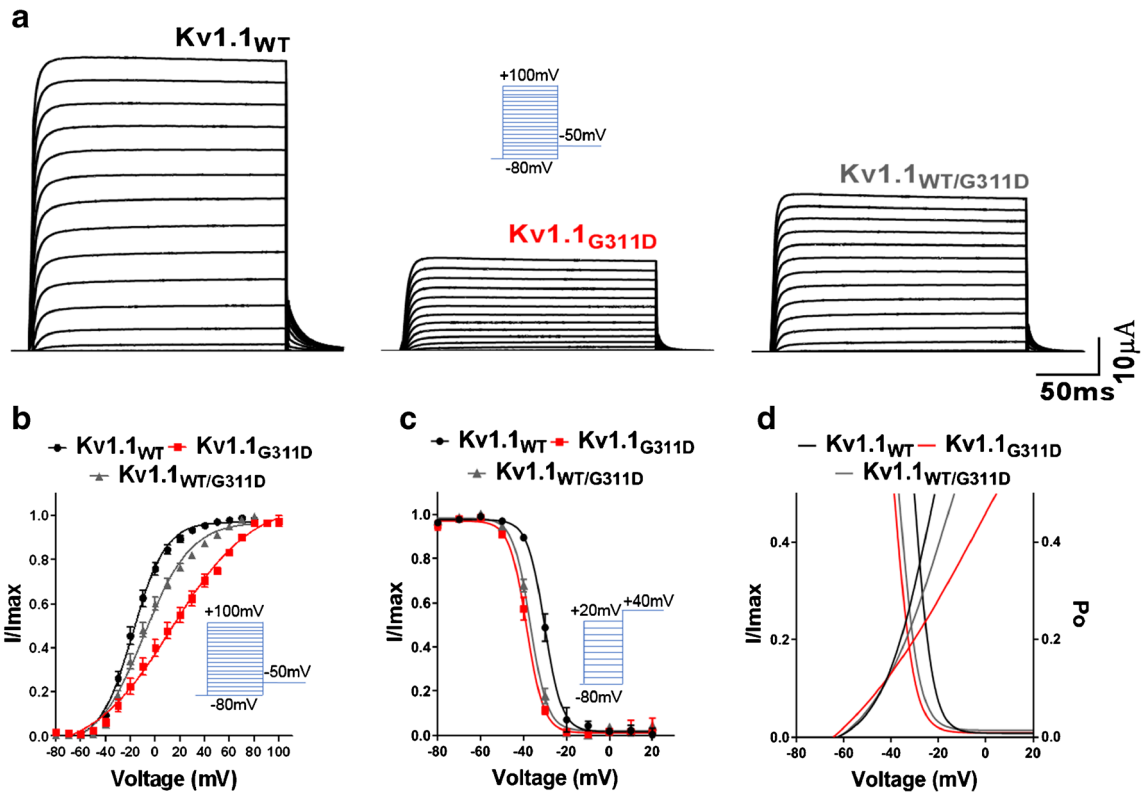

Fig. 2 **a** Representative $Kv1.1_{WT}$, $Kv1.1_{G311D}$, and $Kv1.1_{WT/G311D}$ whole cell current families. Tail currents were recorded at − 50 mV preceded by several pre-pulse voltage commands. **b** Kv1.1 activation (I–V) curves derived from peak amplitudes of tail currents plotted as a function of pre-pulse potentials and fitted with a Boltzmann function. **c** Voltage-dependent inactivation of Kv1.1 channels. Cells were depolarized to various pre-pulse potentials, from − 80 to + 20 mV in + 10 mV increments for 20 s, and then held at + 40 mV test potential for 200 msec. Steady state inactivation curves were derived from the normalization of peak current amplitudes at + 40 mV (I/Imax) and plotted as a function of the pre-pulse potentials. **d** Effect of mutation on window currents, the triangular area under the overlapping point of the activation, and inactivation curves of the respective channel. The calculated areas were WT = 40.0, $Kv1.1_{G311D} = 23.8$, $Kv1.1_{G311D/WT} = 32.3$

to −9 ± 1 mV for the heteromeric $Kv1.1_{WT/G311D}$ channels ($p < 0.0001$, $n = 24$). While the WT curve sharply rises and reaches maximum current within a narrow voltage range, the mutation causes a much more gradual rise. This is correctly represented by the slope factor that increases dramatically for the Kv_{G311D} ($k = 32 \pm 3$, $p < 0.0001$, $n = 24$) and $Kv1.1_{WT/G311D}$ ($k = 19 \pm 1$, $p < 0.0001$, $n = 24$) curves when compared to that of the $Kv1.1_{WT}$ ($k = 13 \pm 0.7$, $n = 24$).

For testing the voltage-dependence of inactivation, oocytes were depolarized to pre-pulse potentials from − 80 to + 20 mV in + 10 mV increments for 20 s, and then held at a + 40 mV test potential for 200 msec. Steady state inactivation curves were derived from normalized peak current amplitudes at + 40 mV (*I*/Imax) plotted as a function of pre-pulse potentials. The mutation left shifted the inactivation curves towards more negative potentials (Fig. 2c). The inactivation curve $V_{0.5}$ of both $Kv1.1_{G311D}$ (− 39 ± 0.5, $n = 10$) and $Kv1.1_{WT/G311D}$ (− 37 ± 0.3, $n = 10$) were statistically different from that of $Kv1.1_{WT}$ (− 30 ± 0.5, $n = 10$, $p < 0.0001$). However, no significant difference was found between the voltage-dependence of the inactivation curves of $Kv1.1_{G311D}$ and $Kv1.1_{WT/G311D}$. Indeed, the slope factors for the inactivation curve were the same for all three groups. The overlapping triangular area between the activation and inactivation curves represents the number of tonically active channels responsible for the window current (Fig. 2d). This area, measured using an integration gadget (OriginLab, Northampton, MA), was 3/5th of that of the WT for $Kv1.1_{G311D}$ and 4/5th of the WT for that of $Kv1.1_{G311D/WT}$ (Fig. 2d).

Changes in kinetics of activation and deactivation

Activation time constants derived from currents recorded as in Fig. 2a were obtained from single exponential fits of the rising phases of test currents. The difference in deactivation rates was examined from a family of tail potentials. Following a depolarizing command to + 40 mV, a family of tail currents was obtained at potentials between − 20 and − 80 mV (Fig. 3). The time course of deactivation was determined by fitting a single exponential function to the tail currents. Time constants were then plotted as a function of membrane potential. Time constants at $V_{0.5}$ ($\tau V_{0.5}$) were derived from the equation $\tau = \tau V_{0.5}\ \exp.\{(V - V_{0.5})/k\}$. While there were no statistical difference between τ of activation at the various voltages from − 10 to + 80 mV, the activation $\tau V_{0.5}$ of the mutant ($Kv1.1_{G311D}$ = 7 ± 0.3 ms, $n = 12$) was half that of the wild type (WT = 14 ± 2 ms, $n = 12$, $p < 0.0005$). $Kv1.1_{G311D/WT}$ was amidst the two latter groups at 9 ± 0.5 ms and was also significantly faster than WT, ($n = 12$, $p < 0.005$). As for deactivation, the mutation resulted in a faster deactivation observed for both $Kv1.1_{G311D}$ and $Kv1.1_{WT/G311D}$ currents ($n = 12$). Deactivation $\tau V_{0.5}$ of the wild type (WT = 19 ± 1 ms, $n = 12$) was significantly greater than that of mutant ($Kv1.1_{G311D}$ = 14 ± 0.9 ms, $n = 12$, $p < 0.005$). There was no significant difference between the $\tau V_{0.5}$ of $Kv1.1_{G311D/WT}$ (19 ± 0.5 ms, $n = 12$) and that of WT.

Changes in slow-inactivation

To determine kinetics of slow inactivation, oocytes were depolarized at + 60 mV for 3.5 min. Representative inactivation currents of $Kv1.1_{WT}$, $Kv1.1_{G311D}$ and $Kv1.1_{WT/G311D}$ were superimposed in Fig. 4a for a clear comparison. The decaying phase of resulting current was fitted with a double exponential. The decaying phase of the $Kv1.1_{G311D}$ current had a smaller fast component contribution when compared to $Kv1.1_{WT}$ ($n = 12$, $p = 0.0004$; Fig. 4b). Nevertheless, τ fast

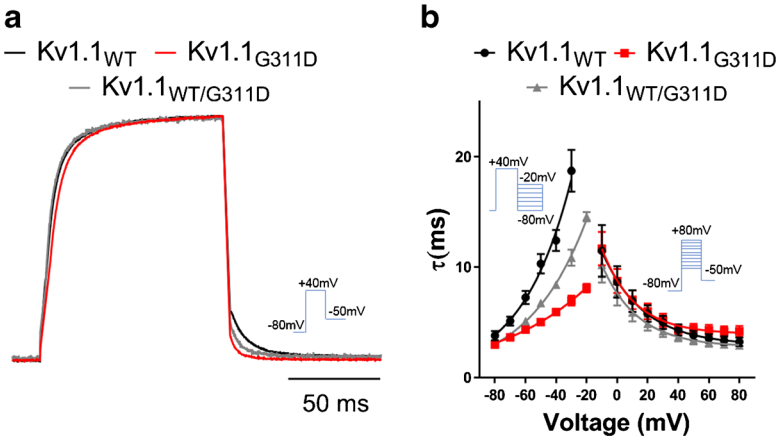

Fig. 3 Activation time constants were obtained from the rising phase of currents elicited by a + 10 mV depolarization steps from a − 80 mV holding potential. Tail currents recorded for 300 ms at − 50 mV were used to obtain deactivation time constants. **a** Normalized and superimposed representative Kv1.1 deactivating currents showing the current from the G311D mutation (red) is the fastest to deactivate. **b** Activating and deactivating current traces were fitted with single exponential functions. Time constants of the currents were plotted as a function of membrane potential. Three plots on the right are activating and the three on the left are deactivating time constants. The data points are mean ± SE of 12 cells

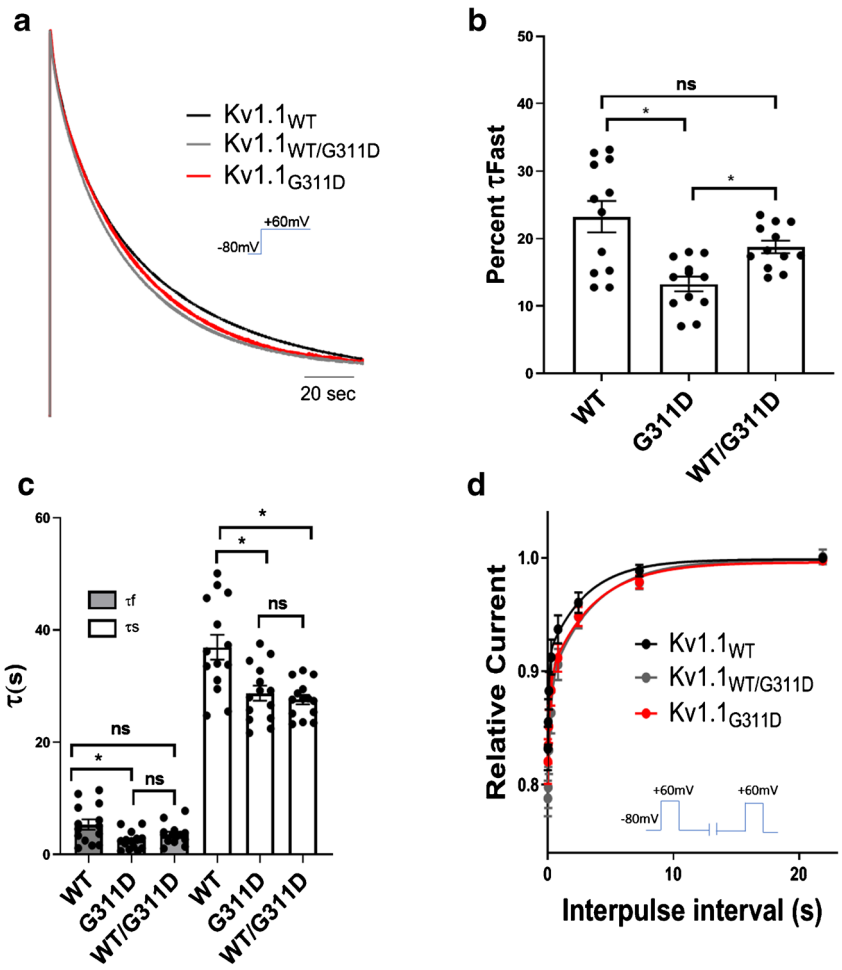

Fig. 4 Kinetics of slow inactivation. **a** Superimposed inactivation currents elicited by depolarization to + 60 mV for 3.5 min. The decaying phase of the current was fitted with a double exponential. **b** Fast component contribution of the decaying phase ($n = 12$). **c** Bar graph showing τfast and τslow of decaying currents ($n = 14$). **d** Normalized peak current amplitudes of currents elicited using a double-pulse recovery protocol were plotted as a function of interpulse interval. The solid lines show the fit with the double exponential function. Data points are mean ± SE of 10 cells

($p = 0.02$, $n = 14$) and τ slow ($p = 0.02$, $n = 14$) were both lower in the $Kv1.1_{G311D}$ currents indicating a faster inactivation (Fig. 4c). In comparison to $Kv1.1_{WT}$, $Kv1.1_{WT/G311D}$ had a lower τ slow; however, there were no significant difference in percent fast component and in τ fast. Recovery from inactivation (refractory period) was measured with a double-pulse protocol of two consecutive 5 s + 60 mV pulses that are separated by interpulse intervals of increasing durations ranging from 0.010 to 21 s. No statistical difference was found in the rate of recovery; thus, the refractory period was not affected by the mutation (Fig. 4d).

Protein structural analysis

The open model of Kv1.1 produced by homology modeling using the template of Kv1.2 as reported by Pathak et al. [19] is in very good agreement with that which we reported previously [9] with only minor differences in external, extracellular loop regions (Fig. 5). The position of the protein in the membrane was examined using the prediction of proteins in membranes (PPM) server [17]. Interestingly, this places the S4-S5 linker helix at the interface of the lower membrane as befitting its amphipathic nature. The hydrophobic side of the helix comprised of three leucine (L312, L315, L319) and two glycine (G311, G316) residues in the wild type is buried within the membrane as is leucine 326 which is part of the S5 helix. The polar side of the helix is formed by lysine 310 and two glutamine (Q313, Q317) residues which reside in the intracellular space. The membrane interface therefore runs along the length of the linker helix. Interestingly, the substitution of G311 with aspartic acid (G311D mutation) does not affect this arrangement of amino acids relative to the membrane (Fig. 5). One factor that may influence this is the ability of D311 to form a bond with K310 (D311 OD2 to K310 NZ is 2.5 Å) (Fig. 5d). Relative to the wild type in which no such bond can exist, this interaction would be expected to neutralize the positive charge of K310 which resides at the bottom of the voltage sensor helix containing several important positively charged residues. In wild-type $Kv1.1_{K310}$ may actually point out of the membrane. Analysis of the similarly generated closed structure (Fig. 5a, c) demonstrates another intriguing interaction of D311, this time with H308. The charge on K310 would in the closed form be left unchanged but the negative charge on the aspartic acid side chain would no longer be shielded by this

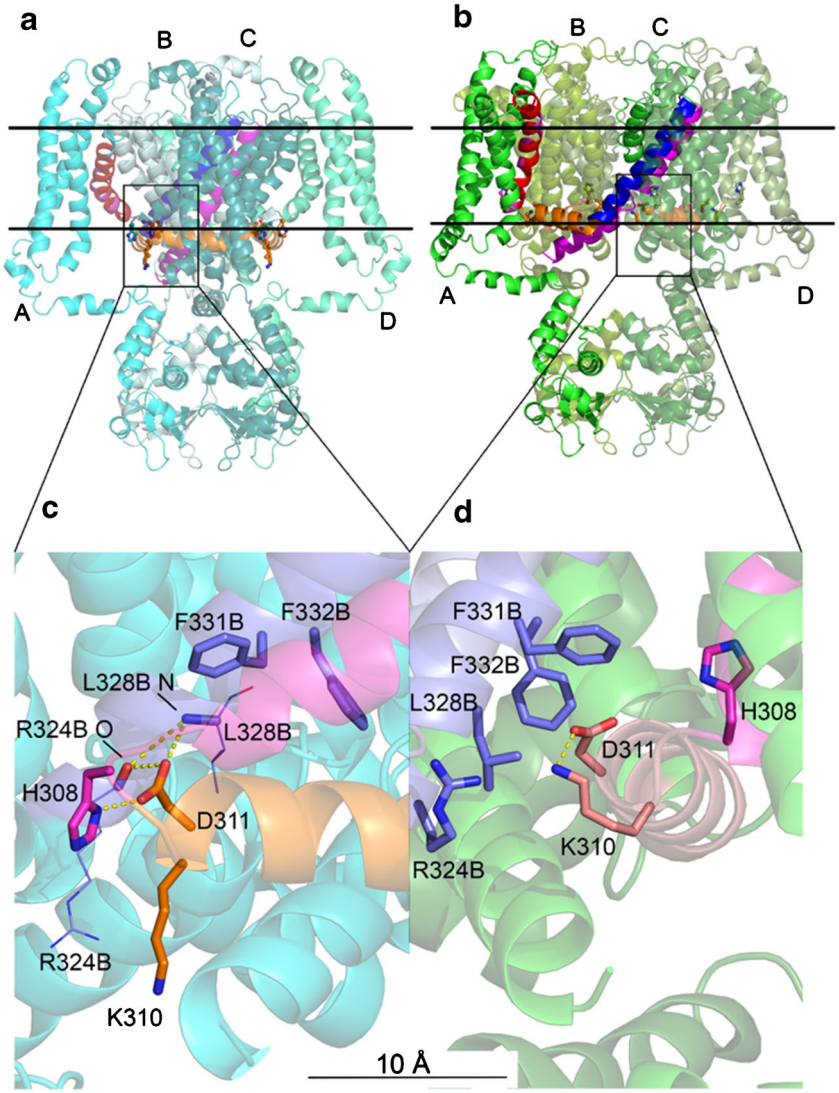

Fig. 5 The predicted structure of Kv1.1-D311 mutant in the closed (**a**, **c**) and open (**b**, **d**) conformations. **a** Closed conformation showing the four polypeptide chains of the tetramer labeled A to D in different shades of blue. **b** Open conformation showing the four polypeptide chains labeled A to D in shades of green. Panels **a** and **b** are shown in the same relative orientation. Thus, the predicted movement of the S4 helix (red, subunit A), S5 helix (blue, subunit A), linker helix (orange, all subunits), and S6 helix (pink) can be readily appreciated. The approximate position of the membrane is shown as horizontal black lines. Panels **c** and **d** show novel interactions of D311 in the closed and open conformations respectively with regions expanded from panels **a** and **b** boxed. Panels **c** and **d** are windows on the same superimposition of the closed and open conformations. Distances as shown are therefore representative of the extents of the conformational change expected. Colors are the same as panels **a** and **b** except the S5 helix (blue) is from a neighboring subunit, B. **c** Closed conformation interactions (yellow dashed lines) between D311 OD1 and H308 ND, and between D311 OD2 and L328 N and R324 O. The latter side chains are drawn as lines for clarity whereas the main chain bonds are drawn as sticks. **d** Open conformation: similarly, interactions between D311 OD1 and K310 NZ. The homologous models were produced using Swiss Model and the Kv1.2 predicted conformations as published by Pathak et al. [19]. Drawings were made using the PyMol molecular viewer

lysine. Instead, it is free to interact with the N atom of the H308 side chain. Both interactions (D311 with K310 in the open form and D311 with H308 in the closed form) would be expected to inhibit the movement of the linker helix from both the open and closed forms. Overall, however, the structure of $Kv1.1_{G311D}$ is not dramatically changed, (Fig. 5).

A similar mutation changing the same glycine residue at position 311 into a serine was previously reported to result in partial *loss-of-function* of Kv1.1 channels and EA1 [22]. The functional characterization of the $Kv1.1_{G311S}$ mutant showed that the voltage dependence of activation for $Kv1.1_{G311S}$ channels was shifted by ~30 mV and the slope of the activation curve was more shallow ($Kv1.1_{G311S}$ $k = 13.4$ vs wild type $k = 8.1$), indicating that $Kv1.1_{G311S}$ has a reduced voltage dependence of activation. The rising phase of $Kv1.1_{G311S}$ currents was best fitted with a single exponential (as for G311D),

yielding a time constant of activation that was slower than the wild type. Furthermore, the time constants for deactivation and slow inactivation were faster for $Kv1.1_{G311S}$ compared to wild type [22]. These biophysical parameters clearly indicate that $Kv1.1_{G311S}$ mirrors the functional properties of $Kv1.1_{G311D}$ channels. Interestingly, the modeling of the $Kv1.1_{G311S}$ mutant showed that similar interactions take place between the hydroxyl side chain of S311 and K310 in the open state (Fig. 6b), but also between this side chain and R324B O, contributed by a neighboring subunit in the predicted closed position (Fig. 6a).

There is considerable conformational change between the open and closed forms as demonstrated by the movement of D311 OD1 by more than 21 Å (Fig. 5c, d). Although highly hypothetical, there is a consensus of agreement that such movement must occur during depolarization and repolarization of the membrane. The glycine residue in the wild type Kv1.1 at position 311 is strategically placed at one end of the linker helix which must bend and slide smoothly past neighboring regions of the protein during the opening and closing of the channel (Figs. 5c, d or 6a, b shows the limits of movement). This is befitting of a glycine residue as its lack of a side chain precludes bonding or sterical clashes with other amino acids. Its substitution by an aspartate introduces a large side chain with accompanying steric hindrance as well as a strong negative charge in a region close to the membrane.

Discussion

Conformational changes responsible for Kv gating, that commence with the sensing of a transmembrane potential change and end with the opening or closing of the channel pore, depend on the S4-S5 linker. In our simulation, the rotation of the linker helix is clearly apparent as is its repositioning relative to other structural elements (Fig. 5). The angle subtended by the S4-S5 linker (orange, Fig. 5) and the S4 helix (red, Fig. 5) increases from around 50° in the closed state to 70° in the open (Pathak et al. [19]). However, little is known about how this linker translates sensor responses to gating conformation. In this study, we characterize the effects of the EA1 G311D mutation located in the intracellular S4-S5. The fact that this glycine is a conserved residue in voltage-dependent potassium channels emphasizes its importance in voltage-dependent gating. We report a *loss-of-function* depicted as reduced current amplitudes and window currents. The window current area (the area under which steady-state activation and inactivation curves intersect) was smaller for the mutant indicating the voltage range within which number of channels that are not inactivated and available for reactivation are smaller. More importantly, we report altered voltage-dependence as the half-maximal activation voltage was shifted nearly 40 mV towards more depolarized potentials. Thus, channels composed of subunits containing the G311D mutation required stronger depolarizations to activate, as indicated also in the positive shifts in heteromeric $Kv1.1_{WT/G311D}$ activation curves compared to WT. Tight coupling between voltage sensing and pore opening results in channel activation that is along a narrow voltage range as indicated in the $Kv1.1_{WT}$ curve in Fig. 1b. The mutation seems to have affected this coupling with a broadening of the depolarizing voltage range before reaching maximal activation. The increase in slope factor of activation is a clear indication of the mutant channel's decreased voltage-dependence. On the other hand, inactivation curves show these channels more readily inactivate at more negative potentials. These findings support the need for therapeutic drugs that target the window area, by shifting voltage-dependent activation and inactivation curves thereby widening the window area and increasing the current.

Co-assembly of mutated subunits with WT subunits usually result in heteromeric channels with biophysical properties somewhere intermediate between that of the channels composed of

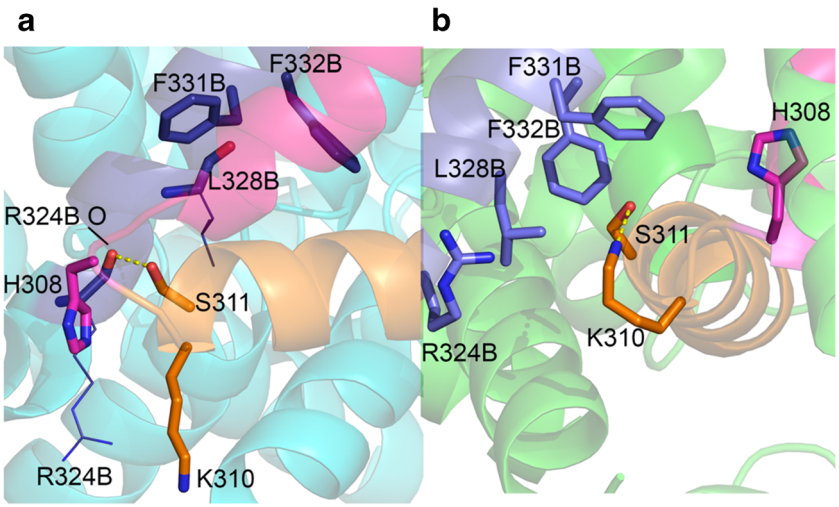

Fig. 6 Predicted interactions of S311 in the closed (**a**) and open (**b**) states. Modeling, colors and residues are as described for Fig. 5

homomeric WT and of homomeric mutant subunits. Our results show that Kv1.1 subunits carrying the mutation can form homomeric $Kv1.1_{G311D}$ channels, albeit with altered kinetics and voltage-dependence. Co-expression results indicate channel properties that lie in-between their homomeric counterparts, suggesting heteromeric channels form altered yet functional channels. However, despite the evidence for changes in gating kinetics and voltage-dependence, decrease in number of channels due to haploinsufficiency cannot be ruled out. The presence of WT subunits along with G311D subunits did not improve the slope or $V_{0.5}$ of the inactivation curve; a dominant-negative effect is thus apparent for the voltage-dependence of inactivation.

Voltage differences across the membrane move positively charged residues within the S4 segment leading to gating conformational changes. While the consensus points to the importance of five positively charged residues (Arg or Lys) that repeat at every third position, the role of the seventh positively charged amino acid K310 that is completely conserved in the Kv1 family has been overlooked.

In the G311D mutant, the presence of the negatively charged D311 at a position adjacent to the seventh cation resulted in the weakening of K310's contribution towards gating charge, hindering S4 (and consequently S4-S5) movement leading to the depolarizing rightward shift and decrease in the channel's voltage-dependence of the observed activation (Fig. 3b). In the open state (Fig. 5d), D311 would bind to K310 masking the effects of the charged residues, and a leftward shift of the inactivation curve is observed that demonstrates a closure that requires less membrane depolarization but with no change in slope indicating the voltage-dependence of inactivation is left unaltered.

The new salt bridge formed between D311and K310, effectively negates their charges. Indeed, if K310 is no longer providing a positive charge (effectively 14% of the total charge on S4), the impetus due to the depolarization of the membrane forcing the conformational change towards the open configuration of the channel will be reduced. While such a bond in the open state would theoretically cause a slowing of the transition to a closed conformation, an acceleration in the deactivation and slow-inactivation processes was observed. It may be possible that due to the loss of positive charge, the fully open state is not achieved or maintained. This could however, be secondary to the dysfunctional voltage-dependent activation. The dysfunctional voltage dependence of activation and the accelerated closure strongly point to a destabilization of the open configuration. A more stable closed configuration that is possible through the D311-H308 bond is likely another contributing factor altering the voltage dependence of activation.

Remarkably, interactions in the modeled G311D are also seen in the G311S mutant between the hydroxyl sidechain of S311 and K310 in the open state, but also between this sidechain and R324B O, in the predicted closed position (Fig. 6). This evidence further supports the conclusion that the presence of a glycine residue at position 311 is essential for proper channel gating.

We have not been able to examine the effect of the membrane phospholipids on this system, other than to predict the most likely limits of the intra- and extra-cellular interfaces. Interestingly, H308 lies fully within these bounds of the membrane in the open state, suggesting that it is not charged and therefore deprotonated. In the closed configuration, however, the side chain of H308 lies on the boundary of the membrane's cytosolic face, a position which is also observed in the original closed model of Kv1.2 [23]. Interactions of H308 with the highly polar phospholipid head groups is a tantalizing possibility and the further effect upon binding with D311 in the $Kv1.1_{G311D}$ mutant, which would bring the negatively charged D311 in proximity of the phospholipids, could be substantial. This might stabilize the closed configuration even more. Movement from the one configuration to the other is quite large, during which the side chain of D311 must contribute some inhibition due to steric hindrance. It could be that movement from open to closed is indeed favored by energetic concerns during transformation from the one conformation to the other.

All *KCNA1* mutations associated with EA1 result in loss of Kv1.1 channel function. Yet each residue mutation has its own signature effect on the channel's biophysical parameters. For example, the mutation $Kv1.1_{R324T}$ located further down along the S4-S5 linker, showed positive shifts in activation and inactivation curves with an insignificant change in slope factor indicating limited effect on voltage dependence [21]. Results of mutagenesis studies suggest that only specific residues in or close to the S4-S5 linker are critical for normal voltage dependence. While some mutations in the Kv1.2 S4-S5 linker (L321F, K322R, M325A, R326K) had indifferent currents and voltage-dependence when compared to that of $Kv1.2_{WT}$, the $Kv1.2_{G329T}$ (that corresponds to $Kv1.1_{G327}$) exhibited positive shifts of $V_{1/2}$ activation and a broadening of the activation voltage range [15]

like that observed in the $Kv1.1_{G311S}$ [22] and the $Kv1.1_{G311D}$ we have studied. A *loss-of-function* accompanied with increased voltage-dependence of activation has been reported for EA1 mutations at locations other than the S4-S5 linker [10, 22]. The *loss-of-function* described in our study is likely responsible for the EA1 symptoms reported for the patients carrying the G311D mutation [10]. In basket cells, a Kv1.1 *loss-of-function* results in longer action potentials and consequently in an enhancement of their Ca^{2+} transients that cause presynaptic increases in γ-aminobutyric acid (GABA) release from their terminals leading to a reduced Purkinje cell inhibitory output [2, 7]. Deep cerebellar nuclei would, as a result, be hyperexcitable, altering cerebellar output and causing the episodic ataxia symptoms characteristic of EA1. Kv1.1 channel *loss-of-function* at juxtaparanodal and axonal branches cause peripheral nerve hyper-excitability resulting in the typical EA1 myokymia symptoms [5, 7, 8, 19, 20].

In conclusion, here, we present evidence for the important role played by a glycine residue within the S4–S5 linker for the voltage-dependent gating of Kv1.1 channels. The changes in the kinetics of activation/deactivation and slow inactivation and the structural analysis we report further confirm a strong effect of the mutation on the channel's gating and stresses the mutation as a cause for the observed symptoms previously reported in the patient.

Materials and methods

Mutagenesis

Kv1.1 human cDNA was subcloned into an oocyte pBF expression vector. Site-directed mutagenesis was performed using QuikChange protocol (Stratagene, La Jolla, CA, USA) and verified by automated sequencing. cRNA was synthesized using "mMESSAGE mMACHINE™ SP6 Transcription Kit (Ambion, Life technologies, Carlsbad, CA, USA). cRNA concentrations were quantified by electrophoresis with ethidium bromide staining and spectrophotometric analysis.

Heterologous expression of KCNA1 constructs

Wildtype ($Kv1.1_{WT}$) and mutant ($Kv1.1_{G311D}$) channels were heterologously expressed in *Xenopus laevis* oocytes as in Hasan et al. [9]. Oocyte extractions were performed in accordance with international standards of animal care, the Maltese Animal Welfare Act and the NIH Guide for the Care and Use of Laboratory Animals. The procedure was approved by the local Veterinary Service Authority. Briefly, oocytes were obtained from *Xenopus laevis* that were deeply anesthetized with an aerated 3-aminobenzoic acid ethyl ester methanesulfonate salt (5 mM) and sodium bicarbonate (60 mM), pH 7.3. Extracted stage V–VI oocytes were digested with Collagenase type A, and each were microinjected with 5 ng/μl, 50 nl cRNA. Homomeric channels composed of four identical WT or four mutated α-subunits, and heteromeric channels composed of both WT and mutated α-subunits were expressed. For heteromeric channels, WT and mutated cRNA were co-injected in a 1:1 ratio (2.5 ng/μl each, 50 nl total volume) in the same oocyte. Oocytes were incubated in ND96 solution (pH 7.4, 16 °C) containing in mM: NaCl 96, KCl 2, $MgCl_2$ 1, $CaCl_2$ 1.8, HEPES 5, and 50 μg/ml gentamicin. Chemicals used in this study were purchased from Sigma-Aldrich.

Electrophysiology

Whole-cell currents were recorded at room temperature (~ 22 °C) from oocytes using the two-electrode voltage-clamp (TEVC) technique in accordance with previously described procedures in Hasan et al. [9]. Currents were measured using a GeneClamp 500 amplifier (Axon Instruments, Foster City, CA) interfaced to a PC computer with an ITC-16 interface (InstruTech, Port Washington, NY). Measurements were taken 48 h after cRNA microinjection. Pulled microelectrodes had a tip resistance of < 1 MΩ when filled with 3 M KCl. The extracellular solution contained (mM): NaCl 96, KCl 2, $MgCl_2$ 1, $CaCl_2$ 1.8, HEPES 5, and pH 7.4. Recordings were analyzed with either PulseFit (HEKA, Germany) or Origin 8 (OriginLab, Northampton, MA). Leak and capacitive currents were subtracted using a P/4 protocol.

Statistical analysis

Prism 7.04 (GraphPad Software, San Diego, CA) was used for statistical analysis. Data are presented as mean ± standard error. Differences were tested using the two-tailed unpaired Student's *t* test, with $p < 0.05$ as the significant value.

Structural analysis

We previously presented an in silico molecular model for the wild-type Kv1.1 potassium channel [9] based on the structure of the Kv1.2 open channel. A similar approach was used to model $Kv1.1_{G311D}$ using the amino acid sequence of the mutant channel and either the open model or the closed model of Kv1.2 [19] as the template for homology modeling utilizing the SWISS-MODEL server [1, 3, 4]. The lowest energy conformer of the D311 mutation (computation in vacuo with the GROMOS69 force field as implemented by Swiss-Pdb Viewer and Swiss-Model) was used, complemented with manual single-bond torsion angle rotation to minimize interaction distances of selected residues (K310 CD-CE by 85.5° in the S311 mutation). Use of the mutant sequence ensured interactions with neighboring subunits would be detected and modeled. To produce Figs. 5

and 6, open and closed forms of the Kv1.1 model were superimposed. Panels 5c and 6a depict the result of the superimpositions with the open conformation removed for clarity. Panels 5d and 6b also depict the result of the superimpositions but with the closed conformation removed for clarity. The extent of motion between open and closed forms is therefore represented by panels 5c and 5d (or 6a and 6b) as drawn in the figures. The predicted membrane-spanning region of both models was explored using the PPM server [16]. Further analyses and molecular images were made using PyMol version 2.3.

Acknowledgments Lorena Coretti is an Alfredo Leonardi's foundation fellow.

Author contributions SH conducted statistics, analyzed the data, prepared the figures, and wrote the article. AM, MC, LC, FMB, and PI conducted molecular biology and electrophysiology experiments. TH and GH did channel modeling and channel structure analysis and contributed in the writing of the paper. HWMS and MP provided advice, consultation, and contributed in writing the paper. MCD planned experimental protocols, coordinated with all authors, supervised the work, and contributed in writing the paper.

Funding information This study is financially supported by the University of Malta Research, Innovation & Development Trust (RIDT) (Grant No. I20LU08, BooKind E20LG42) and of the United Arab Emirates University (Grants Nos. 31M452 and 31M468).

Availability of data and material Derived data supporting the findings of this study are available from the corresponding author CMD on request.

Compliance with ethical standards

Conflict of interest The authors declare that they have no conflicts of interest.

Ethics approval Procedures involving *Xenopus laevis* were in accordance with international standards of animal care, the Maltese Animal Welfare Act, and the NIH Guide for the Care and Use of Laboratory Animals. The procedure was approved by the local Veterinary Service Authority.

Code availability Not applicable.

Consent to participate Not applicable.

Consent for publication Not applicable.

References

1. Arnold K, Bordoli L, Kopp J, Schwede T (2006) The SWISS-MODEL workspace: a web-based environment for protein structure homology modelling. Bioinformatics 22:195–201
2. Begum R, Bakiri Y, Volynski KE, Kullmann DM (2016) Action potential broadening in a presynaptic channelopathy. Nat Commun 7: 12102
3. Biasini M, Bienert S, Waterhouse A, Arnold K, Studer G, Schmidt T, Kiefer F, Gallo Cassarino T, Bertoni M, Bordoli L, Schwede T (2014) SWISS-MODEL: modelling protein tertiary and quaternary structure using evolutionary information. Nucleic Acids Res 42: W252–W258
4. Bordoli L, Kiefer F, Arnold K, Benkert P, Battey J, Schwede T (2009) Protein structure homology modelling using SWISS-MODEL workspace. Nat Protoc 4:1–13
5. Brunetti O, Imbrici P, Botti FM, Pettorossi VE, D'Adamo MC, Valentino M, Zammit C, Mora M, Gibertini S, di Giovanni G, Muscat R, Pessia M (2012) Kv1.1 knock-in ataxic mice exhibit spontaneous myokymic activity exacerbated by fatigue, ischemia and low temperature. Neurobiol Dis 47(3):310–321
6. Bu W, Liang Q, Zhi L, Maciunas L, Loll PJ, Eckenhoff RG, Covarrubias M (2018) Sites and functional consequence of Alkylphenol anesthetic binding to Kv1.2 channels. Mol Neurobiol 55:1692–1702
7. D'Adamo MC, Imbrici P, Sponcichetti F, Pessia M (1999) Mutations in the *KCNA1* gene associated with episodic ataxia type-1 syndrome impair heteromeric voltage-gated K^+ channel function. FASEB J 13(11):1335–1345
8. D'Adamo MC, Liantonio A, Rolland JF, Pessia M, Imbrici P (2020) Kv1.1 channelopathies: pathophysiological mechanisms and therapeutic approaches. Int J Mol Sci 21(8):E2935
9. Hasan S, Bove C, Silvestri G, Mantuano E, Modoni A, Veneziano L, Hunter T, Hunter GJ, Pessia M, D'Adamo MC (2017) A channelopathy mutation in the voltage-sensor discloses contributions of a conserved phenylalanine to gating properties of Kv1.1 channels and ataxia. Sci Rep 7(4583):1–13
10. Hasan SM, D'Adamo MC (2010) Episodic ataxia type 1. Feb 9 [updated 2018 Nov 1]. In: Adam MP, Ardinger HH, Pagon RA et al (eds) GeneReviews® [Internet]. University of Washington, Seattle, Seattle (WA) 1993-2020. Available from: https://www.ncbi.nlm.nih.gov/books/NBK25442/
11. Jensen MØ, Borhani DW, Lindorff-Larsen K, Maragakis P, Jogini V, Eastwood MP, Dror RO, Shaw DE (2010) Principles of conduction and hydrophobic gating in K^+ channels. Proc Natl Acad Sci 107(13):5833–5838
12. Karalok ZS, Megaro A, Cenciarini M, Guven A, Hasan SM, Taskin BD, Imbrici P, Ceylaner S, Pessia M, D'Adamo MC (2018) Identification of a new de novo mutation underlying regressive episodic ataxia type I. Front Neurol 9:587
13. Kuba H, Yamada R, Ishiguro G, Adachi R (2015) Redistribution of Kv1 and Kv7 enhances neuronal excitability during structural axon initial segment plasticity. Nat Commun 6:8815
14. Labro AJ, Raes AL, Grottesi A, Van HD, Sansom MS, Snyders DJ (2008) Kv channel gating requires a compatible S4-S5 linker and bottom part of S6, constrained by non-interacting residues. J Gen Physiol 132:667–680
15. Liang Q, Anderson WD, Jones ST, Souza CS, Hosoume JM, Treptow W, Covarrubias ML (2015) Positive allosteric modulation of Kv channels by sevoflurane: insights into the structural basis of inhaled anesthetic action. PLoS One 10(11):e0143363
16. Lomize MA, Pogozheva ID, Joo H, Mosberg HI, Lomize AL (2012) OPM database and PPM web server: resources for positioning of proteins in membranes. Nucleic Acids Res 40:D370–D376
17. Lomize MA, Pogozheva ID, Mosberg HI (2011) Anisotropic solvent model of the lipid bilayer. 2. Energetics of insertion of small molecules, peptides, and proteins in membranes. J Chem Inf Model 51(4):930–946
18. Long SB, Campbell EB, MacKinnon R (2005) Voltage sensor of Kv1.2: structural basis of electromechanical coupling. Science 309: 903–908
19. Pathak MM, Yarov-Yarovoy V, Agarwal G, Roux B, Barth P, Kohout S, Tombola F, Isacoff EY (2007) Closing in on the resting state of the shaker K^+ channel. Neuron 56(1):124–140
20. Tomlinson SE, Tan SV, Kullmann DM, Griggs RC, Burke D, Hanna MG, Bostock H (2010) Nerve excitability studies

characterize Kv1.1 fast potassium channel dysfunction in patients with episodic ataxia type 1. Brain 133(Pt 12):3530–3540
21. Tristán-Clavijo E, Scholl FG, Macaya A, Iglesias G, Rojas AM, Lucas M, Castellano A, Martinez-Mir A (2016) Dominant-negative mutation p.Arg324Thr in *KCNA1* impairs Kv1.1 channel function in episodic ataxia. Mov Disord 11:1743–1748
22. Zerr P, Adelman JP, Maylie J (1998) Characterization of three episodic ataxia mutations in the human Kv1.1 potassium channel. FEBS Lett 431(3):461–464
23. Zhou L, Messing A, Chiu SY (1999) Determinants of excitability at transition zones in Kv1.1-deficient myelinated nerves. J Neurosci 19(14):5768–5781